NANO LETTERS

pubs.acs.org/NanoLett Letter

Zeta Potential Dependent Self-Assembly for Very Large Area Nanosphere Lithography

Gabriel Cossio and Edward T. Yu*

Cite This: https://dx.doi.org/10.1021/acs.nanolett.0c01277 Read Online

ACCESS | Metrics & More | Article Recommendations | Supporting Information

ABSTRACT: Nanosphere lithography offers a rapid, low-cost approach for patterning of large-area two-dimensional periodic nanostructures. However, a complete understanding of the nanosphere self-assembly process is necessary to enable further development and scaling of this technology. The self-assembly of nanospheres into two-dimensional periodic arrays has previously been attributed solely to the Marangoni force; however, we demonstrate that the ζ potential of the nanosphere solution is critically important for successful self-assembly to occur. We discuss and demonstrate how this insight can be used to greatly increase self-assembled 2D periodic array areas while decreasing patterning time and cost. As a representative application, we fabricate antireflection nanostructures on a transparent flexible polymer substrate suitable for use as a large-area (270 cm^2), broadband, omnidirectional antireflection film.

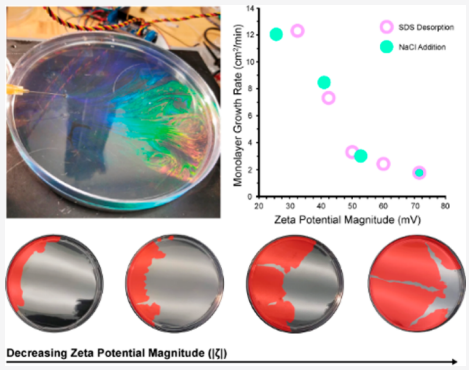

KEYWORDS: *Self-Assembly, Nanosphere Lithography, Antireflection Nanostructures, Zeta Potential, Photovoltaics*

Downloaded via UNIV OF TEXAS AT AUSTIN on June 2, 2020 at 18:25:54 (UTC).
See https://pubs.acs.org/sharingguidelines for options on how to legitimately share published articles.

■ INTRODUCTION

Two-dimensional (2D) periodic nanostructures are employed in a wide range of applications including biomedical device structures,[1,2] nanophotonics,[3,4] renewable energy generation,[5−7] and sensing.[8] Biomimetic 2D periodic nanostructures have demonstrated antifouling,[9] superhydrophobic,[10,11] and antireflection[5−7] properties important to the medical, aviation, and photovoltaic industries. 2D periodic nanostructures have also been proposed for use in subwavelength display pixels,[12−14] transparent and flexible electrodes,[15−19] and broadband metasurface gratings.[20] Unfortunately, the fabrication of these devices can be prohibitively expensive or slow, often requiring state of the art ultraviolet photolithography, electron-beam lithography, or nanoimprint lithography systems. The development of a low-cost, large-area, and scalable patterning method for 2D periodic nanostructures could help address this challenge.

Nanosphere lithography (NSL) is the convective self-assembly of colloidal nanospheres into a lithographic template. Originally demonstrated by Van Duyne et al.,[21] low-cost polystyrene nanospheres (NSs) can be self-assembled into hexagonally close packed (HCP) monolayer arrays and used as lithographic masks. NS arrays can be formed on rigid or flexible substrates. Array periodicity and inclusion dimensions are extremely tunable, as NSs are commercially available with diameters ranging from 10 nm to 10 μm. Hummel et al.[22] have also recently shown that HCP nanosphere monolayers can be transformed into any two-dimensional Bravais lattice, which is important for increasing design flexibility. Recent experiments have demonstrated reproducible 2D nanoparticle monolayers self-assembled from binary colloids, 3D hierarchical nanostructure fabrication, and programmable colloidal molecules, further increasing the design flexibility of NSL.[23−25] However, most reported fabrication areas are limited to cm^2 footprints or smaller, and the theoretical understanding of NSL has remained rudimentary. Recently, Cui et al.[26] proposed a large-area NS self-assembly method for high-throughput 2D periodic nanostructure fabrication. Their micropropulsive injection (MPI) method injects a colloidal solution of NS through a syringe needle onto an air−water interface and can yield very large fabrication areas (m^2), which to our knowledge is the first demonstration of the scalability of NSL. However, a robust explanation for how the NSs are transported from the injected solution onto the air−water interface is still missing. A deeper understanding of NSL's monolayer formation process is still needed in order to minimize defect formation, increase reliability, and reduce fabrication costs and times.

In this study, we demonstrate that the self-assembly of colloidal NSs onto an air−water interface after being injected via a needle tip is strongly dependent on the surface properties of the polystyrene spheres. To achieve this, we prepare colloidal NSs with low-magnitude ζ potential to increase

Received: March 23, 2020
Revised: May 26, 2020
Published: May 28, 2020

 © XXXX American Chemical Society

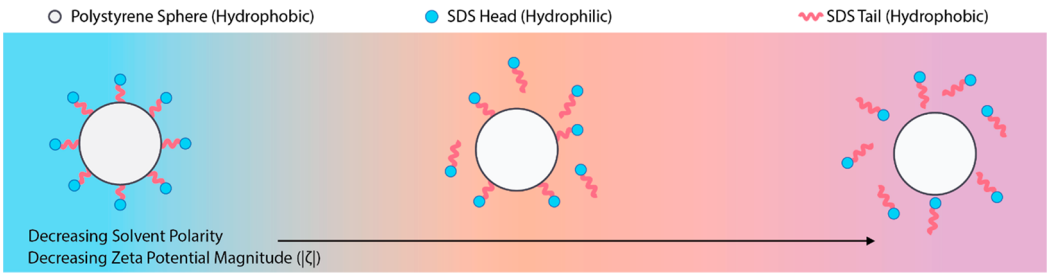

Figure 1. Schematic of surfactant desorption from a polystyrene nanosphere (NS) with decreasing ζ potential magnitude. The nonpolar tails of sodium dodecyl sulfate (SDS) surfactant molecules are adsorbed to the nonpolar polystyrene surface and are repelled from a polar solvent. The polar SDS heads protrude from the NS surface and allow for a stable suspension in a polar solvent. Decreasing the polarity of the solvent allows the NSs to come to a new thermodynamic equilibrium by desorbing a fraction of the SDS molecules into the less polar solvent.

nearest neighbor attraction between NSs and enhance the probability of NSs being promoted to the air−water interface. Moreover, we demonstrate that this effect can be leveraged to improve monolayer formation for different material nanoparticles and thus allows for a greater range of potential applications.

■ RESULTS AND DISCUSSION

Polystyrene NSs are formed by the sequestering and polymerization of styrene monomers inside a surfactant micelle.[27,28] The surfactant micelle therefore defines the geometry of the sphere. The polystyrene NSs used in this study are formed with anionic surfactant molecules, sodium dodecyl sulfate (SDS), on their surfaces. The anionic SDS molecule imparts a negative charge to the sphere, leading to electrostatic and steric repulsion that prevents aggregation. The exposed hydrophilic head prevents flocculation due to repulsive electrostatic forces between spheres and allows the polymer spheres to be extremely stable in aqueous solutions. By resuspending polymer NSs in solvents that are less polar than water, it becomes energetically more favorable for the hydrophobic tail of the surfactant to expose itself, promoting desorption of surfactant molecules from the NS surface as illustrated schematically in Figure 1. When NSs that have desorbed some fraction of their surfactant molecules are then placed back in water, the repulsive electrostatic forces between spheres are greatly reduced. This is due to the decrease in electrostatic repulsion arising from the negatively charged sulfate groups of the SDS molecule. The exposed hydrophobic surface of the spheres will then prefer to be near other hydrophobic surfaces (nearby spheres) instead of their polar aqueous environment. As will be shown, this strategy for decreasing repulsive forces between NSs is not limited to polystyrene NSs. In fact, NSs with different surface chemistries can be functionalized to enhance attractive forces between NSs and thereby increase self-assembly efficiency. For example, SiO_2 NSs can also be functionalized with a cationic surfactant, hexadecyltrimethylammonium bromide (CTAB), in order to facilitate self-assembly.

By measuring the ζ potential of a colloidal dispersion, we can implicitly measure the stability of a suspension of NSs. The ζ potential is a measurement of the electric potential difference between the slipping plane of a nanoparticle and the bulk of

Table 1. Washing of Polystyrene Nanospheres in Different Solvents[a]

solvent	ζ potential magnitude (mV)	standard deviation (mV)
DI water	71.50	7.95
25% EtOH	59.15	6.75
100% IPA	54.70	6.91
50% acetone	50.60	8.55
100% EtOH	49.70	7.54
50% acetone, 50% EtOH	42.80	5.47
100% acetone	32.40	5.27

[a]The ζ potential is negative due to the anionic sulfate group which forms the hydrophilic head of the SDS surfactant molecule. Washing in solvents of lower polarity causes more SDS to desorb from the NS surface. Once decanted, there is less SDS present, and the magnitude of the ζ potential is lowered.

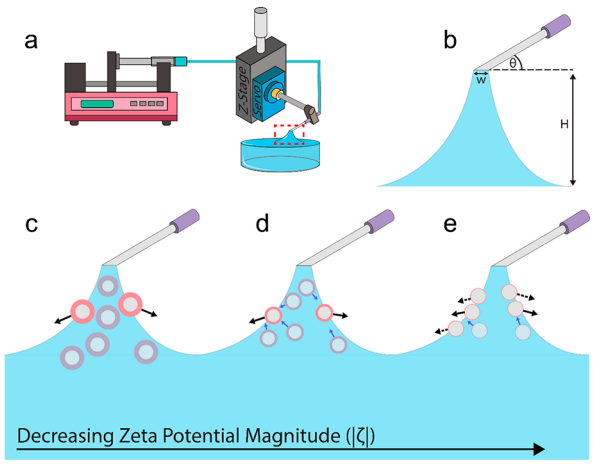

Figure 2. (a) Schematic of the injection system for NS monolayer formation on the surface of a water reservoir. A syringe pump drives the NS solution into a needle that forms a meniscus at the air−water interface. (b) Close-up of the meniscus formed between the needle and water. The height of the meniscus (H) and injection angle (θ) are controlled by a micrometer stage and servo motor, respectively. The minimum meniscus width (w) is controlled by the needle gauge. (c−e) Schematic illustration of a physical model of the self-assembly process at different ζ potential magnitudes: (c) NSs injected into solutions with high ζ potential magnitude are prevented from getting to close to each other due to strong electrostatic repulsions (represented as a thick pink shell around NSs). (d) As the ζ potential magnitude is decreased, the electrostatic repulsion between spheres is weakened (thinner pink shell around NSs), and NSs can increase in proximity thereby increasing the probability that NSs will collectively escape to the surface of the air−water interface and contribute to NS monolayer formation. (e) NSs in very low magnitude ζ potential solutions NSs may be in very close proximity and cluster to NSs that are exiting the meniscus, further increasing their escape probability.

https://dx.doi.org/10.1021/acs.nanolett.0c01277
Nano Lett. XXXX, XXX, XXX−XXX

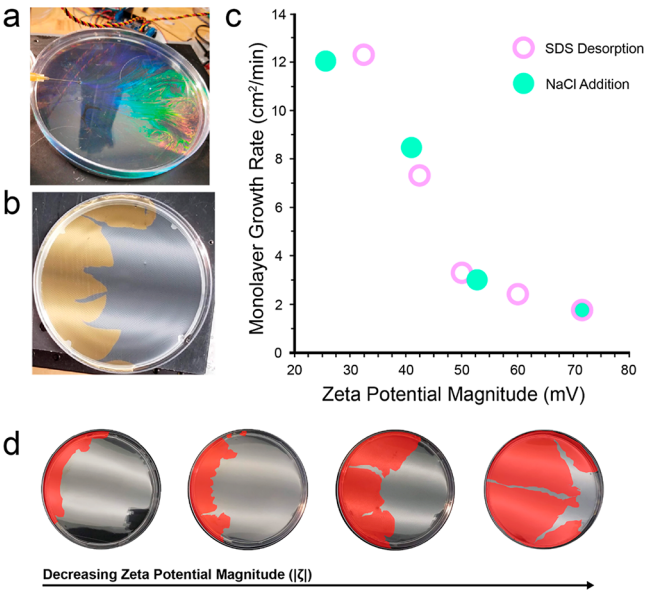

Figure 3. (a) Injection of 200 nm polystyrene NSs. Iridescent reflections appear as NSs are injected onto the water's surface. (b) Image of a 200 nm HCP monolayer formed on the surface of water via NS injection. The 200 nm polystyrene monolayer is the region on the left side of the reservoir that appears orange on the surface of water. (c) Monolayer growth rate as a function of ζ potential magnitude. Solutions tested were made either by desorption of SDS (pink) or by addition of NaCl (green). (d) Images of self-assembled monolayers of 200 nm diameter polystyrene NSs from solutions of decreasing magnitude ζ potential. (71.5 mV, 50.6 mV, 42.8 mV, 32.4 mV) from left to right, respectively. False color (red) is used to highlight the monolayer areas.

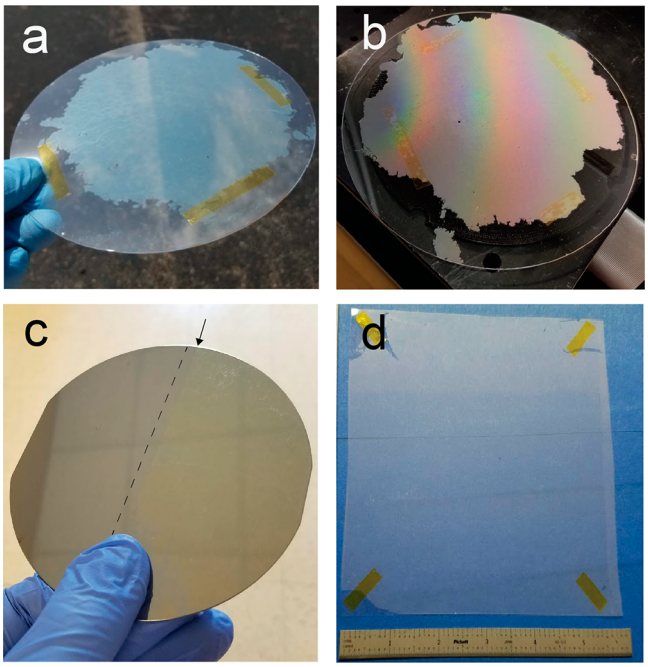

Figure 4. (a) 200 nm polystyrene NS monolayer deposited on 6" diameter polycarbonate wafer. (b) 2 μm polystyrene NS monolayer deposited on 6" diameter polycarbonate wafer. (c) 200 nm SiO_2 NS monolayer deposited on 4" diameter Si wafer. The monolayer appears slightly yellow in hue and is to the right of the dotted line. The arrow marks the edge of the monolayer. (d) 270 cm^2 polymer sheet (PET) coated with a monolayer of 200 nm polystyrene NSs. The NS monolayer appears white.

the solvent. Therefore, a high-magnitude ζ potential implies that the nanoparticles in solution are highly charged relative to their suspended environment, while the sign of the ζ potential indicates whether the particles are negatively or positively charged. Table 1 shows the decrease in the magnitude of the ζ potential from polystyrene spheres as they are washed in different solvents. As can be seen from Table 1, as the polystyrene NSs are repeatedly washed in solvents that are less polar than water, the magnitude of the NSs' ζ potential decreases. We attribute this decrease in the magnitude of the ζ potential to the decrease in the concentration of SDS molecules that are still adsorbed to the surface of the NS, as illustrated schematically in Figure 1. Measurements and solutions were prepared as described in the Supporting Information. These solutions were used for monolayer growth rate measurements and appear as the SDS desorption data points in Figure 3c.

Figure 2a,b shows schematics of our nanosphere injection apparatus and the needle-reservoir interface, respectively. During the injection process, a NS solution (preparation described in Supporting Information) is first pumped to an injecting needle which forms a meniscus at an air−water interface. Injection parameters and colloidal solution details are described in the Supporting Information. Our physical model of the injection and self-assembly process is as follows. The meniscus acts as a transporting region where the injected NSs can move from the meniscus volume to the air−water interface, a low-probability event that occurs when the NSs have the correct position and velocity vector (positioned near the meniscus and moving toward interface). Only NSs that reach the air−water interface at the reservoir surface can contribute to NS monolayer formation. The injected NSs have a wide initial distribution of position and velocity vectors that are functions of diffusion, convection, and other variables. The analysis of these initial positions and velocities is beyond the scope of this paper. We assume that the distribution of initial positions and velocities across different injections is identical so long as the same contact angle, flow rate, meniscus height, and injection width are maintained. Consistent with this assumption, we observed highly reproducible, uniform, high-quality monolayer film formation across 5" × 5" areas during successive depositions onto flexible PET substrates, and across multiple other trials (Figure S1 in the Supporting Information).

Figure 2c−e illustrates schematically how decreasing the ζ potential magnitude can increase the likelihood of NSs escaping the meniscus, a critical step for NS self-assembly on an air−water interface. When the injecting solution has a high ζ potential magnitude (Figure 2c), the NSs in the meniscus are strongly repelled from each other due to strong electrostatic and steric repulsion. This is depicted in the figure as the large pink shell around each NS that prevents the NSs from getting closer together. As a result, the NSs act independently, and only NSs with the ideal position and velocity can escape the meniscus and reach the air−water interface. In Figure 2c, only two NSs have the ideal placement and velocity to escape the meniscus, shown as the brighter NSs (above the water's surface) with the black arrows pointing out and down the meniscus. When the ζ potential magnitude is lowered (Figure 2d), the repulsive forces are reduced (thinner pink shell), and submerged NSs may begin to aggregate (blue arrows) to NSs

https://dx.doi.org/10.1021/acs.nanolett.0c01277
Nano Lett. XXXX, XXX, XXX−XXX

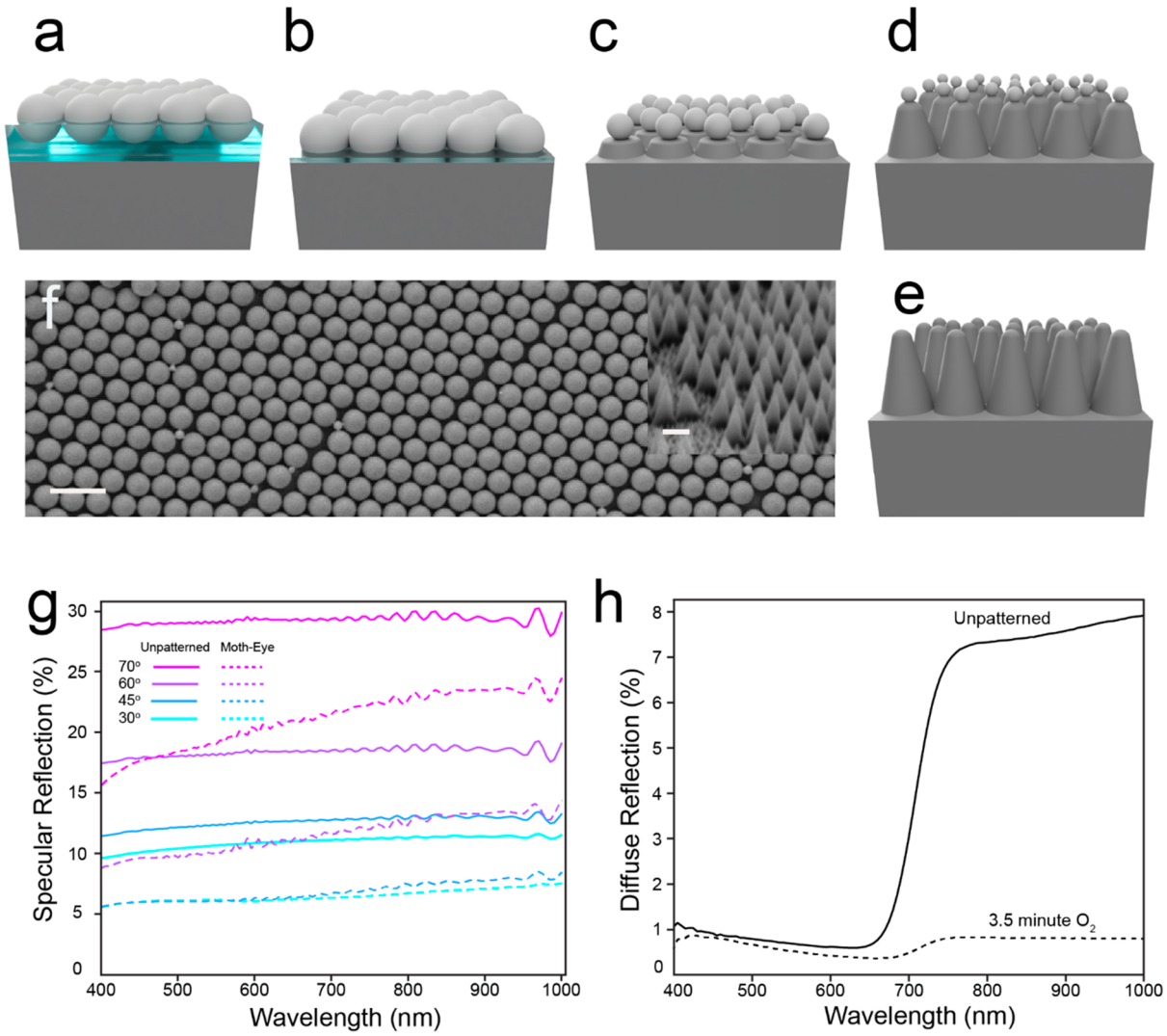

Figure 5. (a−e) Schematic illustration of the moth-eye nanostructure fabrication process. (f) SEM image of 200 nm NS monolayer. Scale bar is 500 nm. The inset shows an image of fabricated moth-eye antireflection nanostructures. Scale bar is 200 nm. (g) Measured angular dependent specular reflection from unpatterned PET film (solid line) and moth-eye patterned film (dashed line). Moth-eye textured film was made with 3.5 min of O_2 etching. (h) Diffuse reflectance from PET films etched for 3.5 min in O_2 plasma.

that are escaping the meniscus. Further reducing the ζ potential magnitude (Figure 2e) lowers electrostatic and steric repulsions enough that NSs can get close enough to produce strong attractive van der Waals forces. NSs that aggregate toward a NS that is escaping the meniscus now have a higher probability of escaping as they are all clustered together. These secondary ejections (black dotted line) are only possible when strong clustering is favorable. NSs that make it to the air−water interface are in a lower-energy configuration and therefore cannot be pulled back into the bulk water volume. For this reason, NSs on the air−water interface act as a low-energy trap that enables movement of NSs that are in solution and close to the air−water interface onto the air−water interface so as to minimize their free energy. After NSs have escaped to the air−water interface, the Marangoni force[29] (created from the surface tension difference between the solvent in the injected solution and the surface tension of the surrounding deionized (DI) water) pulls the NSs down the meniscus surface and away from the injected area. This may facilitate further secondary ejections of NSs as NSs that have escaped the meniscus volume and are bound to the air−water interface move past and continue to interact with NSs that are submerged and near the air−water interface.

Figure 3a shows a solution of 200 nm diameter NSs (prepared by SDS desorption as described in the Supporting Information) being injected onto an air−water interface via the meniscus formed between the needle tip and DI water surface. This injection method leads initially to formation of a disordered array of NSs. At the start of the injection, very few NSs are at the air−water interface, which continues to appear transparent. Eventually, an iridescent reflection appears due to diffraction from a loosely packed NS monolayer floating on the surface. Continuing the injection increases the density of the NSs on the air−water interface and decreases the separation between NSs. For 200 nm polystyrene NSs, the iridescence is gradually replaced by a single prominent orange reflection (Figure 3b), which is to be expected as the separation between spheres reaches subwavelength dimensions, and diffractive reflection is suppressed. The change in reflected light marks the point in the injection at which the NS monolayer is approaching HCP densities. After this point is reached, one drop of 0.5 mL of 10% SDS is added to one edge

https://dx.doi.org/10.1021/acs.nanolett.0c01277
Nano Lett. XXXX, XXX, XXX−XXX

of the monolayer. The high concentration of SDS greatly lowers the surface tension at the point of impact, and the Marangoni force drives the monolayer to the side opposite the SDS addition (where the surface tension is the highest). The strong Marangoni force causes the NSs to be packed into an HCP arrangement. Figure 3b shows an HCP monolayer of 200 nm polystyrene NSs on an air−water interface after the addition of 0.5 mL of 10% SDS.

Figure 3c shows the effect of ζ potential magnitude on self-assembly efficiency. All solutions were injected for 10 min onto the surface of Milli-Q DI water in a 6" Petri dish. All injection variables, except for the ζ potential of the NSs, were held constant (see the Supporting Information). The ζ potential of the injected solutions was varied by desorption and decanting of SDS molecules (pink) or by addition of NaCl (green). After 10 min of injection, a 0.5 mL droplet of 10% SDS was dropped onto the edge of the surface. The area of the monolayer is calculated from a captured image, and the average rate of increase corresponding to the final monolayer area is reported in Figure 3c. As can be seen from Figure 3c, as the magnitude of the ζ potential is decreased, NSs are more efficiently transported out of the meniscus and onto the surface of the water, evident by enhanced monolayer growth areas (Figure 3d, shown in false color). The monolayer growths by SDS desorption presented in Figure 3c were completed by washing of polystyrene NSs in DI water, 25% ethanol, 50% acetone, 50% acetone, 50% ethanol, and 100% acetone. The magnitudes of the ζ potential of the injection solutions after these solvent washing procedures were lowered to 71.50, 59.15, 50.60, 42.80, and 32.40 mV, respectively. By lowering the magnitude of the ζ potential of 200 nm polystyrene NSs to approximately 30 mV, we achieve a maximum monolayer growth rate of 12.2 cm^2/min and surface coverage of 79% (144 cm^2). The lowest growth rate and percent coverage, 1.80 cm^2/min and 12% (21 cm^2), are achieved when the magnitude of the ζ potential is the highest, 71.5 mV.

It is important to note that, even at the highest ζ potential magnitude, when NSs are most hydrophilic and least likely to minimize their energy by escaping onto the air−water interface, there is still measurable monolayer formation. This implies that some fraction of NSs have the correct velocity and orientation imparted to them from diffusion. However, relying on these effects for monolayer formation alone is inefficient. We also note that the Marangoni force on the surface of the meniscus should be identical for both high- and low-magnitude ζ potential solutions. This is because the amount of ethanol across solutions is not being changed, and Marangoni forces arise due to the surface tension gradient between the ethanol and water. Therefore, the Marangoni force is not the key variable for promoting NSs to the air−water interface as previously reported. However, its role as a spreading agent is critical and prevents aggregation at the point of injection.

We expect that the maximum efficiency of NS transport from the meniscus volume onto the surface of water occurs when NSs are injected through a meniscus with very high surface to volume ratio and a low ζ potential magnitude. A meniscus with high surface to volume ratio will allow NSs to navigate through the least amount of water volume before finding the air−water interface. The lower the magnitude of the ζ potential, the lower the repulsion between NSs. The resulting increase in proximity between NSs should increase the probability of secondary ejection from the meniscus, in which NSs that happen to be near a NS that is escaping the meniscus get "pulled" out of the meniscus due to the attractive van der Waals forces between NSs.

In order to further understand the mechanisms that increase the monolayer formation efficiency, we performed a set of injections in which the ζ potential was instead tuned via addition of NaCl. This way, the ζ potential can be varied by changing the amount of charge in solution and effectively lowering the electric potential between the NSs and the solvent by screening the charge on the NS surface (from the negatively charged adsorbed SDS) without affecting the hydrophobicity of the NSs. Figure 3c shows the monolayer formation rate when the ζ potential is tuned via addition of NaCl (green circles) versus SDS desorption (pink circles). ζ potential measurements of solutions containing additional NaCl can be found in Table S1 of the Supporting Information. As can be seen in Figure 3c, similar behavior in the monolayer formation efficiency is seen when the ζ potential is changed via the addition of NaCl. This suggests that the most important parameter in increasing the efficiency of monolayer formation is particle−particle interactions such as van der Waals attraction between NSs. Both solutions (i.e., produced by either SDS desorption or NaCl addition) are characterized by increasing van der Waals attraction between NSs as the magnitude of the ζ potential is lowered. However, only the solution prepared via desorption of SDS has NSs whose surface becomes increasingly hydrophobic as the magnitude of the ζ potential is decreased (due to exposure of the hydrophobic polystyrene core). We can therefore deduce that there is a negligible effect on the monolayer formation efficiency from the exposure of the hydrophobic surface of the sphere, and the critical variable for enhancing monolayer formation efficiency is NS proximity.

To demonstrate the versatility of this self-assembly method, NS monolayers were fabricated using different sizes of NSs and also using different materials. Figure 4a,b shows monolayers formed by polystyrene NSs with diameters of 200 nm and 2 μm, respectively, and deposited on a flexible polycarbonate wafer 6" in diameter. Figure 4c shows a monolayer of 200 nm silica nanospheres deposited onto a 4" silicon wafer. The silica monolayer appears yellow in hue and covers the area of the wafer to the right of the dashed line. The black arrow highlights the edge of the silica NS monolayer. Tape was used to mask off the left half of the wafer to increase contrast between the pure silicon side and the monolayer covered side. SEM images, as well as further discussion of the 2 μm polystyrene and 200 nm silica NS self-assembled monolayers, are available in the Supporting Information (Supplementary Note 1 and Figure S3).

Figure 4d shows a 270 cm^2 area PET sheet that is covered with a monolayer of 200 nm polystyrene NS. The formation of this large-area monolayer shows that, by using our enhanced injection method, further scaling of nanosphere lithography is possible. To illustrate a representative application, we used the deposited 270 cm^2 monolayer area as a lithographic mask to fabricate moth-eye antireflection nanostructures. The omnidirectional and broadband antireflection properties of moth-eye nanostructures are important for optoelectronic applications, such as antireflection surfaces for photovoltaics and photodetectors. Figure 5a−e shows a schematic of the moth-eye fabrication process. First, NSs are self-assembled at the air−water interface (Figure 5a) via the previously described injection method. The NS monolayer is then drained onto a polymer substrate (Figure 5b). The polystyrene NSs and

https://dx.doi.org/10.1021/acs.nanolett.0c01277
Nano Lett. XXXX, XXX, XXX−XXX

polymer substrate are then etched simultaneously in an O_2 plasma. Continuous etching shrinks the NSs and reveals previously masked areas of the substrate. As more of the substrate is revealed, and the NSs continue shrinking, a high aspect ratio moth-eye nanostructure is formed (Figure 5c–e). Figure 5f shows an SEM image of the 200 nm NS monolayer formed on the PET sheet surface (scale bar 500 nm), and the inset shows the fabricated moth-eye nanostructures (scale bar 200 nm).

Figure 5g shows the angle dependent specular reflection from an unpatterned (solid lines) flexible PET film and the same film with the moth-eye nanopattern texturing (dashed lines). Angle of incidence (AOI) was measured relative to the surface normal of the sample with 0° and 90° being perpendicular and parallel incidences, respectively. Measurements were taken at 30°, 45°, 60°, and 70° AOI between 400 and 1000 nm. Samples with moth-eye textures were etched for 3.5 min in an O_2 plasma. As expected, moth-eye textured sheets show a broadband reduction in specular reflection. Averaging across the spectrum shows that specular reflections from moth-eye textured films are 4.44%, 4.91%, 5.91%, and 7.28% lower than the untextured films for 30°, 45°, 60°, and 70° AOI respectively. PET sheets with moth-eye antireflection nanopatterning appear clearer with a reduction in glare. Photographs of the PET sheets with and without moth-eye nanopatterning can be seen in Figure S4. Diffuse reflectance measurements (Figure 5h) were also taken to ensure that the decrease in specular reflectance also corresponds to a decrease in total reflection. Etch conditions were optimized to minimize specular and diffuse reflectance. Diffuse reflectance from an unpatterned PET film (solid black line) reaches as high as 7.9% in the long wavelength region and 4.0% average diffuse reflectance across the entire spectrum. After adding the moth-eye texturing to the PET films, the average diffuse reflectance is lowered to 0.6% reaching a maximum of 0.8% at 420 nm.

In conclusion, a new, detailed explanation for the self-assembly behavior of NS monolayers via needle injection is presented and verified. We show that, in contrast to previous descriptions, the Marangoni force is not the only key variable that contributes to the escape of NSs from an injecting meniscus onto an air–water interface. Instead, the tendency of NSs to be positioned in close proximity to each other, as quantified by the ζ potential magnitude, is a crucial variable in enabling the scaling of self-assembly techniques. By decreasing the ζ potential magnitude of an injected NS solution, we are able to increase the monolayer growth rate from 1.8 to 12.2 cm^2/min and monolayer growth areas by 6.85×. We believe attractive van der Waals forces between NSs increases particle proximity and can lead to a secondary ejection of NSs from the meniscus onto the air–water interface. Large monolayer areas were used to make large-area, subwavelength antireflection moth-eye nanostructures on flexible polymer films. These films show superior broadband and omnidirectional performance, decreasing diffuse reflection from 4% for unpatterned films to 0.8% for moth-eye nanotextured films and specular reflection from 28% to 21% for large angles of incidence (70°).

■ ASSOCIATED CONTENT

Supporting Information

The Supporting Information is available free of charge at https://pubs.acs.org/doi/10.1021/acs.nanolett.0c01277.

Procedures for preparation of colloidal solutions, experimental parameters, fabrication of moth-eye nanostructures, photographs and SEM images of various self-assembled NS monolayers, and discussion of the silica NS self-assembly (PDF)

■ AUTHOR INFORMATION

Corresponding Author

Edward T. Yu – *Department of Electrical and Computer Engineering, The University of Texas at Austin, Austin, Texas 78758, United States*; Email: ety@ece.utexas.edu

Author

Gabriel Cossio – *Department of Electrical and Computer Engineering, The University of Texas at Austin, Austin, Texas 78758, United States*; orcid.org/0000-0001-6706-7726

Complete contact information is available at: https://pubs.acs.org/10.1021/acs.nanolett.0c01277

Notes

The authors declare no competing financial interest.

■ ACKNOWLEDGMENTS

This work was performed in part at the University of Texas Microelectronics Research Center, a member of the National Nanotechnology Coordinated Infrastructure (NNCI), which is supported by the National Science Foundation grant (ECCS-1542159). The authors acknowledge the use of facilities and instrumentation supported by the National Science Foundation through the Center for Dynamics and Control of Materials: an NSF MRSEC under Cooperative Agreement DMR-1720595. Part of this work was supported by the Army Research Laboratory (Dr. Charles Rong). We would also like to thank Dr. Ryan Klein, Steven Stanley, and Professor Roger Bonnecaze for helpful discussions.

■ REFERENCES

(1) Ivanova, E. P.; Hasan, J.; Webb, H. K.; Truong, V. K.; Watson, G. S.; Watson, J. A.; Baulin, V. A.; Pogodin, S.; Wang, J. Y.; Tobin, M. J.; Lobbe, C.; Crawford, R. J. Natural bactericidal surfaces: mechanical rupture of Pseudomonas aeruginosa cells by cicada wings. *Small* **2012**, *8* (16), 2489–2494.

(2) Campoccia, D.; Montanaro, L.; Arciola, C. R. A review of the biomaterials technologies for infection-resistant surfaces. *Biomaterials* **2013**, *34* (34), 8533–8554.

(3) Kempa, K.; Kimball, B.; Rybczynski, J.; Huang, Z. P.; Wu, P. F.; Steeves, D.; Sennett, M.; et al. Photonic crystals based on periodic arrays of aligned carbon nanotubes. *Nano Lett.* **2003**, *3* (1), 13–18.

(4) Chen, K.; Rajeeva, B. B.; Wu, Z.; Rukavina, M.; Dao, T. D.; Ishii, S.; Aono, M.; Nagao, T.; Zheng, Y. Moiré nanosphere lithography. *ACS Nano* **2015**, *9* (6), 6031–6040.

(5) Li, X.; Li, P.-C.; Ji, L.; Stender, C.; McPheeters, C.; Tatavarti, S. R.; Sablon, K.; Yu, E. T. Subwavelength nanostructures integrated with polymer-packaged iii–v solar cells for omnidirectional, broad-spectrum improvement of photovoltaic performance. *Prog. Photovoltaics* **2015**, *23* (10), 1398–1405.

(6) Li, X. H.; Li, P. C.; Hu, D. Z.; Schaadt, D. M.; Yu, E. T. Light trapping in thin-film solar cells via scattering by nanostructured antireflection coatings. *J. Appl. Phys.* **2013**, *114* (4), 044310.

(7) Huang, Y.-F.; Chattopadhyay, S.; Jen, Y.-J.; Peng, C.-Y.; Liu, T.-A.; Hsu, Y.-K.; Pan, C.-L.; Lo, H.-C.; Hsu, C.-H.; Chang, Y.-H.; Lee, C.-S.; Chen, K.-H.; Chen, L.-C. Improved broadband and quasi-omnidirectional anti-reflection properties with biomimetic silicon nanostructures. *Nat. Nanotechnol.* **2007**, *2* (12), 770.

(8) Haes, A. J.; Van Duyne, R. P. A nanoscale optical biosensor: sensitivity and selectivity of an approach based on the localized surface plasmon resonance spectroscopy of triangular silver nanoparticles. *J. Am. Chem. Soc.* **2002**, *124* (35), 10596−10604.
(9) Kim, P.; Kreder, M. J.; Alvarenga, J.; Aizenberg, J. Hierarchical or not? Effect of the length scale and hierarchy of the surface roughness on omniphobicity of lubricant-infused substrates. *Nano Lett.* **2013**, *13* (4), 1793−1799.
(10) Barthlott, Wilhelm; Neinhuis, Christoph Purity of the sacred lotus, or escape from contamination in biological surfaces. *Planta* **1997**, *202* (1), 1−8.
(11) Liu, K.; Yao, X.; Jiang, L. Recent developments in bio-inspired special wettability. *Chem. Soc. Rev.* **2010**, *39* (8), 3240−3255.
(12) Gawlik, B. M.; Cossio, G.; Kwon, H.; Jurado, Z.; Palacios, B.; Singhal, S.; Alu, A.; Yu, E. T.; Sreenivasan, S. V. Structural coloration with hourglass-shaped vertical silicon nanopillar arrays. *Opt. Express* **2018**, *26* (23), 30952−30968.
(13) Nagasaki, Y.; Suzuki, M.; Hotta, I.; Takahara, J. Control of Si-based all-dielectric printing color through oxidation. *ACS Photonics* **2018**, *5* (4), 1460−1466.
(14) Kim, I.; Yoon, G.; Jang, J.; Genevet, P.; Nam, K. T.; Rho, J. Outfitting next generation displays with optical metasurfaces. *ACS Photonics* **2018**, *5* (10), 3876−3895.
(15) Morfa, A. J.; Akinoglu, E. M.; Subbiah, J.; Giersig, M.; Mulvaney, P. Transparent metal electrodes from ordered nanosphere arrays. *J. Appl. Phys.* **2013**, *114* (5), 054502.
(16) Gao, T.; Huang, P.-S.; Lee, J.-K.; Leu, P. W. Hierarchical metal nanomesh/microgrid structures for high performance transparent electrodes. *RSC Adv.* **2015**, *5* (87), 70713−70717.
(17) van de Groep, J.; Spinelli, P.; Polman, A. Transparent conducting silver nanowire networks. *Nano Lett.* **2012**, *12*, 3138−3144.
(18) Xu, X.; Kwon, H.; Gawlik, B.; Mohammadi Estakhri, N.; Alù, A.; Sreenivasan, S.V.; Dodabalapur, A. Enhanced photoresponse in metasurface-integrated organic photodetectors. *Nano Lett.* **2018**, *18* (6), 3362−3367.
(19) Zhang, L.; Zhong, X.; Pavlica, E.; Li, S.; Klekachev, A.; Bratina, G.; Ebbesen, T. W.; Orgiu, E.; Samori, P. A nanomesh scaffold for supramolecular nanowire optoelectronic devices. *Nat. Nanotechnol.* **2016**, *11* (10), 900.
(20) Mohammadi Estakhri, N.; Argyropoulos, C.; Alù, A. Graded metascreens to enable a new degree of nanoscale light management. *Philos. Trans. R. Soc., A* **2015**, *373* (2049), 20140351.
(21) Hulteen, J. C.; Van Duyne, R. P. Nanosphere lithography: A materials general fabrication process for periodic particle array surfaces. *J. Vac. Sci. Technol., A* **1995**, *13* (3), 1553−1558.
(22) Hummel, M. E. J.; Stelling, C.; Kopera, B. A. F.; Nutz, F. A.; Karg, M.; Retsch, M.; Forster, S. Ordered Particle Arrays via a Langmuir Transfer Process: Access to Any Two-Dimensional Bravais Lattice. *Langmuir* **2019**, *35* (4), 973−979.
(23) Lotito, V.; Zambelli, T. Self-assembly of single-sized and binary colloidal particles at air/water interface by surface confinement and water discharge. *Langmuir* **2016**, *32* (37), 9582−9590.
(24) Xu, X.; Yang, Q.; Wattanatorn, N.; Zhao, C.; Chiang, N.; Jonas, S. J.; Weiss, P. S. Multiple-patterning nanosphere lithography for fabricating periodic three-dimensional hierarchical nanostructures. *ACS Nano* **2017**, *11* (10), 10384−10391.
(25) Ni, S.; Leemann, J.; Buttinoni, I.; Isa, L.; Wolf, H. Programmable colloidal molecules from sequential capillarity-assisted particle assembly. *Science advances* **2016**, *2* (4), No. e1501779.
(26) Gao, P.; He, J.; Zhou, S.; Yang, X.; Li, S.; Sheng, J.; Wang, D.; Yu, T.; Ye, J.; Cui, Y. Large-area nanosphere self-assembly by a micro-propulsive injection method for high throughput periodic surface nanotexturing. *Nano Lett.* **2015**, *15* (7), 4591−4598.
(27) Antonietti, M.; Bremser, W.; Mueschenborn, D.; Rosenauer, C.; Schupp, B.; Schmidt, M. Synthesis and size control of polystyrene latices via polymerization in microemulsion. *Macromolecules* **1991**, *24* (25), 6636−6643.
(28) Schwuger, M.-J.; Stickdorn, K.; Schomaecker, R. Microemulsions in technical processes. *Chem. Rev.* **1995**, *95* (4), 849−864.
(29) Scriven, L. E.; Sternling, C. V. The marangoni effects. *Nature* **1960**, *187* (4733), 186−188.

https://dx.doi.org/10.1021/acs.nanolett.0c01277
Nano Lett. XXXX, XXX, XXX−XXX